FOOD FRONTIERS Open Access

RESEARCH ARTICLE OPEN ACCESS

Structural Characterization, Phenolic Acid Modification, and Antioxidant Activities of Polysaccharide From Mogroside Waste Liquid of *Siraitia grosvenorii*

Jiajing Duan | Yufeng Sun | Bo Wang | Qinfei Xie | Yang Ju | Fengzhong Wang | Bei Fan

Institute of Food Science and Technology, Chinese Academy of Agricultural Sciences/Key Laboratory of Agroproducts Quality and Safety Control in Storage and Transport Process, Ministry of Agriculture and Rural Affairs, Beijing, China

Correspondence: Fengzhong Wang (wangfengzhong@sina.com) | Bei Fan (fanbei517@163.com)

Received: 11 October 2024 | **Revised:** 16 January 2025 | **Accepted:** 5 February 2025

Funding: This research was supported by the National Key Research and Development Plan (2022YFD1600303, 2022YFC2010104).

Keywords: antioxidant | modification | phenolic acid | *Siraitia grosvenorii* polysaccharide | structure

ABSTRACT

To improve the comprehensive utilization of *Siraitia grosvenorii* (Swingle) C. Jeffrey, a novel polysaccharide (SGP) was isolated from the mogroside waste liquid of *S. grosvenorii*. In addition, ferulic acid–SGP (FA-SGP) and caffeic acid–SGP (CA-SGP) were prepared by modifying SGP with phenolic acid. The structural characteristics and antioxidant activities of the three polysaccharides were analyzed. SGP displayed a pore-like structure and was mainly composed of glucose and xylose with a molecular weight of 2.64 kDa. It was a pyran-type polysaccharide with both α-glycosidic and β-glycosidic bonds. The linkage types were Glcp-(1→D →3)-Glcp-(1→, →4)-Glcp-(1→, →6)-Glcp-(1→, →3,6)-Glcp-(1→. FA and CA were covalently attached to SGP by ester bonds, and the molecular weights of FA-SGP and CA-SGP were 5.34 and 3.83 kDa, respectively. They formed a tightly interconnected reticulation structure. Activities tests demonstrated that compared to the native SGP, FA-SGP and CA-SGP could significantly enhance the antioxidant capacity and improve the protective effects on H_2O_2-damaged SH-SY5Y cells. The regulation of FA-SGP and CA-SGP toward the oxidative stress in SH-SY5Y cells might be related to the Bcl-2/Caspase-3/Bax signaling pathways. In this study, phenolic acid grafts with excellent antioxidant activity were prepared using SGP as the lead compound. This provided a new direction for obtaining *S. grosvenorii* products with satisfactory bioactivity and a reference for the deep processing of *S. grosvenorii* industry.

1 | Introduction

Siraitia grosvenorii (Swingle) C. Jeffrey is a perennial vine plant of the Cucurbitaceae family. It is mainly distributed in Lingui and Yongfu in the Guangxi Zhuang Autonomous Region of China, accounting for over 90% of the world's production. In 2002, *S. grosvenorii* was recognized as one of the top medicinal and food species in China, with high nutritional and medicinal values (Duan et al. 2023). *S. grosvenorii* polysaccharide (SGP) is demonstrated with various bioactivities, such as antioxidant, hypoglycemic, antitumor, and immune effects (Zhu et al. 2020). Gong et al. (2023) found that SGP was useful in the removal of 1,1-diphenyl-2-picrylhydrazyl radical 2,2-diphenyl-1-(2,4,6-trinitrophenyl) hydrazyl (DPPH•),

Jiajing Duan and Yufeng Sun contributed equally to this paper.

This is an open access article under the terms of the Creative Commons Attribution License, which permits use, distribution and reproduction in any medium, provided the original work is properly cited.

© 2025 The Author(s). *Food Frontiers* published by John Wiley & Sons Australia, Ltd and Nanchang University, Northwest University, Jiangsu University, Zhejiang University, Fujian Agriculture and Forestry University.

2,2′-azinobis-(3-ethylbenzthiazoline-6-sulfonate) (ABTS•), and hydroxyl radical (OH•), demonstrating excellent antioxidant activity. They also found that SGP treatment could increase the glycogen content of IR-HepG2 cells, indicating good hypoglycemic activity (Gong et al. 2022). Zhang et al. (2019) found that SGP treatment could ameliorate spleen tissue damage induced by cyclophosphamide, indicating excellent immune function. Currently, *S. grosvenorii* is mostly used to extract the natural sweetener, mogroside. The waste liquid containing sugar generated in the production of mogroside is mainly used to produce alcohol through fermentation. However, SGP with multiple bioactivities in the mogroside waste liquid is often ignored. Thus, the rational utilization of SGP is of great significance for development of *S. grosvenorii* industry.

The activity of polysaccharides is highly dependent on structural features. The different modification groups can directly or indirectly affect their activity or pharmacological effects (Li et al. 2023; Fillaudeau et al. 2024; Esposito et al. 2024; Hashemi et al. 2024). Thus, new bioactive derivatives can be obtained by modifying the structure, molecular weight (M_w), and substituent groups of polysaccharides (Tan et al. 2019). Sulfation is the main modification method in SGP. Gong et al. (2023) prepared the sulfated derivative S-SGP (M_w: 13.4 kDa) using the chlorosulfonic acid method, demonstrating in vitro antioxidant and antitumor activity. Phenolic acids, a class of non-flavonoid polyphenols widely found in plants, are natural antioxidants. It can not only inhibit the activity of free radicals by utilizing the phenolic hydroxyl group in its structure to provide active hydrogen, but it also increases the activity of intracellular antioxidant enzymes such as superoxide dismutase (SOD) and catalase (CAT), thus exerting excellent antioxidant effects in the organism (Shi et al. 2024). Ferulic acid (FA) and caffeic acid (CA), originating from the phenylalanine biological metabolic pathway, are hydroxycinnamic acid derivatives (Bao et al. 2018). They exist in a free or bound state in nature. Their molecules have double bonds and short alkyl chains, endowing them with excellent biological activities such as antioxidant, antimicrobial, and anti-inflammatory properties. They have broad application prospects in the food, medicine, and cosmetics fields (Liu et al. 2014). Studies have shown that phenolic acid modification could enhance the bioactivities of other substances (Hu et al. 2020; Hu et al. 2023). Phenolic acid–modified polysaccharides can endow polysaccharides with enhanced or unique biological activities. Ma et al. (2019) grafted maltodextrin with FA, which showed improved antioxidant activity compared to native maltodextrin. Wang et al. (2019) grafted chitosan with CA, resulting in enhanced antioxidant activity compared to native chitosan. However, limited research has been done on SGP phenolic acid modification.

In this study, a novel SGP was isolated from mogroside waste liquid. Phenolic acid–modified derivatives of FA-SGP and CA-SGP were prepared using a free radical–mediated method, which was economical and environment-friendly. Their structures were characterized by scanning electron microscopy (SEM), ultraviolet (UV) spectroscopy, Fourier transform infrared (FT-IR) spectroscopy, and nuclear magnetic resonance (NMR) spectroscopy. The antioxidant activities were investigated through the determination of DPPH•, OH•, and ABTS• radical–scavenging effects, as well as the protective effects against oxidative stress in human neuroblastoma cells (SH-SY5Y), which were damaged by H_2O_2. This study provides a reference for phenolic acid modification and the total utilization of *S. grosvenorii*.

2 | Materials and Methods

2.1 | Materials and Reagents

Mogroside waste liquid was obtained after extraction of mogroside. DEAE-52 cellulose, glucose standard solution, bovine serum protein standard solution, glucose, xylose, arabinose, rhamnose, mannose, galactose, glucuronic acid, ascorbic acid, Congo red, L-ascorbic acid (Vc), sodium hydroxide (NaOH), FA, CA, and salicylic acid were purchased from Shanghai Yuanye Biotechnology Co. Ltd. (China). Phenol, concentrated sulfuric acid, trichloroacetic acid, 95% ethanol, dichloromethane (DCM, CH_2Cl_2), and hydrogen peroxide (H_2O_2) were purchased from Sinopharm Chemical Reagent Co. Ltd. (China). Cell counting kit-8 (CCK-8), phosphate buffered saline (PBS), bicinchoninic acid assay (BCA) kit, malondialdehyde (MDA) kit, and total SOD activity assay were purchased from Solepol Technology Co. Ltd. (China). SH-SY5Y complete culture medium was purchased from Wuhan Shangen Biotechnology Co. Ltd. (China). DMEM medium, 0.25% Trypsin-EDTA, was purchased from Thermo Fisher Scientific. DPPH• was purchased from Sigma. ABTS• kit was purchased from Nanjing Jiancheng Biotechnology Co. Ltd. (China). B-cell lymphoma-2 (Bcl-2), Bcl-2–associated X protein (Bax), and Caspase-3 were purchased from ABCAM.

2.2 | Extraction of SGP

Crude SGP was extracted from the mogroside waste liquid through high-temperature deproteinization and alcohol precipitation. Briefly, the mogroside waste liquid (20 g) was mixed with 95% ethanol (60 mL). The mixture was allowed to stand at 4°C for 24 h. The precipitate was collected and freeze-dried to afford crude SGP. It was purified by ion exchange chromatographic purification. Briefly, crude SGP (0.1 g) was dissolved in distilled water (100 mL) and poured slowly to a cellulose DEAE-52 column (2.6 cm × 70 cm). Then, it was eluted using distilled water with a flow rate of 5 mL/min. The elution products were collected (5 mL/tube) consecutively, and the carbohydrate content was detected one by one with phenol–sulfuric acid colorimetric method (Mondal et al. 2001). The collection was stopped until no carbohydrate was eluted out. The elution curve was plotted according to the optical density (OD) value of eluate in each tube at 490 nm. The purified fractions were concentrated, dialyzed with distilled water at 4°C for 48 h, and freeze-dried to afford refined SGP. The residual nucleic and protein were checked by UV full wavelength scanning in the range of 200–400 nm (Mondal et al. 2001).

2.3 | Determination of Total and Reducing Sugar Content in SGP

The total sugar content in SGP was determined by phenol–sulfuric acid colorimetric method (Gong et al. 2023). Specifically, a 1.0 mg/mL glucose standard solution was prepared and

subsequently diluted with distilled water to 0.02, 0.04, 0.06, 0.08, and 0.10 mg/mL. A total of 1 mL of the above working solutions were mixed with 5% phenol solution (0.5 mL) and 98% sulfuric acid (2.5 mL). Then, the reaction was conducted at 100°C for 30 min. Afterward, the absorbance of each resulting solution at a wavelength of 490 nm was measured and used to establish a standard curve. Finally, the absorbance of 0.04 mg/mL SGP treated solution following the above procedures was measured and used to calculate the total sugar content in SGP according to the established standard curve.

The reducing sugar content in SGP was determined by 3,5-dinitrosalicylic (DNS) acid colorimetric method. Briefly, the above glucose working solutions (1 mL) were mixed with DNS reagent (1 mL). Then, the reaction was conducted at 100°C for 5 min. Afterward, the mixtures were diluted with distilled water (8 mL). The absorbance of each resulting solution at a wavelength of 540 nm was measured and used to establish a standard curve. Finally, the absorbance of 0.04 mg/mL SGP treated solution following the above procedures was measured and used to calculate the reducing sugar content in SGP according to the established standard curve.

2.4 | Monosaccharide Composition Analysis of SGP

The determination of monosaccharide composition of SGP was carried out according to previous method (Cheng et al. 2020). Specifically, SGP (10 mg) was hydrolyzed with trifluoroacetic acid under nitrogen protection at 120°C for 4 h. The residual acid was removed by nitrogen blowing. The product was dissolved in ultrapure water (10 mL) and diluted to 20 folds. The solution was filtered through a 0.2 μm membrane and separated on a CarboPacTMPA20 (3 mm × 150 mm, Dionex, USA) at 35°C, with integrated a pulsed amperometric detector. The mobile phases comprised three solvents: A (water), B (250 mmol/L NaOH solution), and C (1 mol/L sodium acetate). This mobile phase system was run at 0.5 mL/min, and the gradient elution condition was set as follows: 0%–94% A, 0%–6% B (0–20 min); 94%–89% A, 6% B, 0%–5% C (20–20.1 min); 89%–74% A, 6% B, 5%–20% C (20.1–35 min); 74%–20% A, 6%–80% B, 20%–0% C (35–35.1 min); 20% A, 80% B (35.1–45 min); 20%–94% A, 80%–6% B (45–45.1 min); 94% A, 6% B (45.1–55 min). The monosaccharides were analyzed by external calibration with an equimolar mixture of eight monosaccharide standards (fucose, rhamnose, arabinose, galactose, glucose, xylose, fructose, galacturonic acid, and glucuronic acid).

2.5 | Methylation Analysis of SGP

The methylation analysis was conducted according to the method of previous reports (Gao et al. 2020a; Hou et al. 2023) with some modifications. Specifically, SGP (3 mg) was dissolved in dimethyl sulfoxide (1 mL), followed by a quick addition of methylation reagent A (NaOH solution) and B (iodomethane solution). The reaction was conducted at 30°C for 1 h and stopped by addition of ultrapure water (2 mL). Subsequently, hydrolysis was carried out for 1.5 h with addition of trifluoroacetic acid (1 mL, 2 mol/L). Then, reduction was conducted for 8 h with addition of double-distilled water (2 mL) and sodium borohydride (60 mg). The solution was neutralized using glacial acetic acid and dried at 101°C. Finally, acetylation was carried out at 100°C for 1 h with addition of acetic anhydride (1 mL). The resulting solution was added with toluene (3 mL), concentrated to remove residual acetic anhydride, and extracted with DCM (3 mL) for four times. The product was fixed to 10 mL and analyzed using an Agilent 6890-5973 GC–MS system with a RXI-5 SIL MS column (30 m × 0.25 mm × 0.25 μm). The oven conditions were set at initial temperature of 120°C and increased to 250°C at a rate of 3°C/min, and held for 5 min. Both the inlet temperature and the detector temperature were 250°C. The carrier gas was helium, and the flow rate was 1 mL/min. The test was repeated three times.

2.6 | Molecular Weight Analysis of SGP

The molecular weight distribution of SGP used gel exclusion chromatography (DAWN HELEOS II, Wyatt, USA) equipped with OHpak SB-803 HQ column (8 mm × 300 mm, Shodex, Japan) and refractive index detector (RID-20A). The column was set at 40°C and eluted with 0.05 mol/L sodium chloride solution at a speed of 0.8 mL/min. The sample (25 μL, 5 mg/mL) was analyzed with dextran as a reference, and the retention time (RT) and standard molecular weight were recorded.

2.7 | Phenolic Acid Modification of SGP

A free radical–mediated method was used to prepare FA-modified SGP (Liu et al. 2013). Specifically, SGP (0.5 g) was dissolved in 0.5% acetic acid solution (50 mL), followed by addition of Vc (0.1 g) and FA (0.8 g). The mixture was stirred under nitrogen protection at 25°C for 30 min, followed by addition of hydrogen peroxide solution (2 mL, 5 mol/L). The reaction was continued under nitrogen protection at 25°C for 12 h. The result solution was dialyzed with distilled water at 4°C for 72 h. Finally, the dialysate was freeze-dried to afford FA-SGP (yield: 70.1 mg). The same method was used to prepare CA-SGP (yield: 50.2 mg). Their molecular weight was determined in Section 2.6. Their purities were estimated by UV full wavelength scanning in the range of 260–400 nm.

2.8 | SEM Observation of SGP, FA-SGP, and CA-SGP

The microstructures of SGP, FA-SGP, and CA-SGP were observed using an SEM (SU8010, Hitachi, Japan). Briefly, the conductive adhesive was pasted on the sample stage, coated with powdered SGP, FA-SGP, and CA-SGP (2 mg, respectively), and sputtered with gold powder. The carrier stage was placed inside the SEM. The microstructures were observed by adjusting the magnification (Guo et al. 2023).

2.9 | FT-IR Analysis of SGP, FA-SGP, and CA-SGP

SGP, FA-SGP, and CA-SGP (1 mg) were mixed with potassium bromide powder (100 mg), respectively, ground and pressed into a disc (1 mm). The spectra were recorded using an FT-IR

spectrophotometer (TENSOR 27, Bruker, USA) in the range of 500–4000 cm^{-1} (Deng et al. 2020).

2.10 | NMR Analysis of SGP, FA-SGP, and CA-SGP

SGP, FA-SGP, and CA-SGP (15 mg) were dissolved in deuteroxide (500 μL), respectively, and transferred to NMR tubes. Subsequently, ^{1}H NMR (600 Hz) and ^{13}C NMR (150 Hz) spectra of each sample were recorded using an NMR spectrometer (JEOL ECS-400, JEOL, Japan) and analyzed with MestReNova software (Cheng et al. 2020).

2.11 | Determination of Free Radical–Scavenging Ability

2.11.1 | DPPH• Radical Scavenging Assay

The DPPH• radical scavenging assay was conducted according to previous research with some modifications (Chen et al. 2019). SGP, FA-SGP, and CA-SGP (5 mg) were dissolved in distilled water and diluted to varying concentrations (0.05, 0.1, 0.2, 0.4, 0.8, and 1.0 mg/mL). The solutions (1 mL) were mixed with 1 mL of DPPH• (0.2 mmol/L in ethanol) and incubated in the dark at 25°C for 30 min. A control sample containing the DPPH• solution without the sample was also prepared. In the blank, the DPPH• solution was substituted with ethanol (Zhang et al. 2022; Wang et al. 2022). Then, the absorbance values of each resulting solution were measured at 517 nm using UV spectrophotometer (UV-9000, Shanghai Metasch Instruments Co. Ltd., China). Although FA and CA have excellent antioxidant activity, they were not selected as positive control due to their poor water solubility. However, the same concentration of Vc was taken as a positive control. The antioxidant activity of the sample was evaluated using the inhibition percentage of the DPPH• with the following equation:

$$\text{DPPH}\bullet\ \text{radical} - \text{scavenging activity}\ \ (\%) = \left[1 - \frac{A_1 - A_2}{A_0}\right] \times 100$$

where A_0 represents the OD value of the mixture of 50% ethanol and DPPH•, A_1 represents the OD value of the mixture of sample, and A_2 represents the OD value of the mixture of sample and ethanol.

2.11.2 | OH• Scavenging Assay

The OH• scavenging activity was determined by the Fenton method (Chen and Huang 2019). SGP, FA-SGP, and CA-SGP (5 mg) were dissolved in distilled water and diluted to varying concentrations (0.05, 0.1, 0.2, 0.4, 0.8, and 1.0 mg/mL). The solutions (1 mL) were mixed with ferrous sulfate solution (1 mL, 9 mmol/L), hydrogen peroxide solution (1 mL, 8.8 mmol/L), and salicylic acid solution (1 mL, 9 mmol/L in ethanol), and incubated in the dark at 25°C for 1 h. Then, the absorbance values of each resulting solution were measured at 510 nm using a UV spectrophotometer. Distilled water and Vc were taken as blank control and positive control, respectively. The OH• scavenging activity was determined as follows:

$$\text{OH}\bullet\ \text{scavenging activity}\ \ (\%) = \left[1 - \frac{A_1 - A_2}{A_0}\right] \times 100$$

where A_0 represents the OD value of distilled water, A_1 represents the OD value of the mixture of sample, and A_2 represents the OD value of distilled water instead of salicylic acid.

2.11.3 | ABTS• Scavenging Assay

The ABTS• scavenging assay was conducted according to previous research with some modifications (Zhang et al. 2021; Zhou et al. 2011). SGP, FA-SGP, and CA-SGP (5 mg) were dissolved in distilled water and diluted to varying concentrations (0.05, 0.1, 0.2, 0.4, 0.8, and 1.0 mg/mL). The ABTS• scavenging activity was determined using the ABTS• reagent kit with the antioxidant trolox as standard and expressed as Trolox-equivalent antioxidant capacity (TEAC):

$$\text{TEAC}\ (\text{mM}) = -1.1214 \times A + 1.1262$$

where A represents the OD value of the mixture of sample.

2.12 | Cell Viability Assay

The frozen SH-SY5Y cells were resuscitated at 37°C and resuspended in DMEM cell culture medium containing 10% fetal bovine serum and 1% penicillin–streptomycin. The mixture was centrifuged at 2000 rpm for 3 min. The SH-SY5Y cells were incubated in an incubator with a carbon dioxide concentration of 5% and a temperature of 37°C. The SH-SY5Y cells undergone passaging culture were selected and inoculated into a 96-well plate (5×10^4 cells/100 μL cell suspension/well), followed by incubation. Subsequently, the wells were added with SGP, FA-SGP, and CA-SGP solution to achieve final concentrations of 0, 50, 100, 200, 400, and 800 μg/mL, respectively, and placed in incubator for 48 h. Afterward, the wells were added with CCK-8 solution (10 μL) and placed in incubator for 1 h. The absorbance value of each well was measured at 450 nm using a full wavelength scanning enzyme labeler (Spectra MAX190, Molecular devices), and the cell viability was calculated (Zheng et al. 2024).

2.13 | Cell Model Construction

Cell model, H_2O_2-damaged SH-SY5Y cells, was constructed according to previous research (Jin and Wang 2019). The SH-SY5Y cells undergone passaging culture were selected and inoculated into a 96-well plate (5×10^4 cells/100 μL cell suspension/well), followed by incubation. Subsequently, the wells were added with H_2O_2 solution to achieve final concentrations of 0, 50, 100, 200, 400, and 800 μmol/L, respectively, and placed in incubator for 24 h. Afterward, the wells were added with CCK-8 solution (10 μL) and placed in incubator for 1 h. The absorbance value of each well was measured at 450 nm, and the cell viability was calculated.

2.14 | Experiment on the Protective Effect on Cell Model

The SH-SY5Y cells undergone passaging culture were selected and inoculated into a 96-well plate (5×10^4 cells/100 μL cell suspension/well), followed by incubation. Low-dose group (100 μg/mL), medium-dose group (200 μg/mL), and high-dose group (400 μg/mL) containing SGP, FA-SGP, and CA-SGP were set, as well as the control group (Con) without polysaccharide and model group (M) with H_2O_2 solution (200 μmol/L). The groups were incubated for 24 h and added with H_2O_2 solution (200 μmol/L), followed by incubation for another 24 h. Afterward, the wells were added with CCK-8 solution (10 μL) and placed in incubator for 1 h. The absorbance value of each well was measured at 450 nm, and the cell viability was calculated.

2.15 | Measurement of Oxidative Stress-Related Indicators and Western Blotting

Based on Section 2.14, the control group, model group, and medium-dose group (200 μg/mL) were selected to measure the oxidative stress-related indicators, SOD and MDA. Briefly, the cells of the groups were collected and lysed using RIPA lysis buffer (containing PMSF). The mixture was centrifuged at 12,000 rpm at 4°C for 5 min, and the supernatant was used for determination of the content of SOD and MDA according to the instructions of the kit. Then, the western blotting was conducted. Specifically, the proteins in the above supernatant were separated by sodium dodecyl sulfate–polyacrylamide gel electrophoresis (SDS-PAGE) and then transferred to polyvinylidene fluoride (PVDF) membrane for 1 h at a constant current of 300 mA. The membranes were sequentially incubated with primary antibody (Bcl-2, Bax, Caspase-3, and GAPDH), secondary antibody (goat anti-rabbit IgG), and enhanced chemiluminescence (ECL) solution, followed by autoradiography. The intensity of the blot was analyzed by Image pro plus 6.0.

2.16 | Statistical Analysis

All experiments were conducted in triplicate. Data were expressed as mean ± standard deviation (SD) and analyzed using GraphPad Prism statistical software (8.0.1).

3 | Results and Discussion

3.1 | Total and Reducing Sugar Content in SGP

The crude *S. grosvenorii* polysaccharide was purified using a DEAE-52 cellulose column with distilled water as an eluent. The elution curve is shown in Figure 1A. This indicated that DEAE-52 cellulose column displayed a good separation from SGP. The UV full wavelength scanning spectrum of the refined SGP is shown in Figure 1B. No absorption peaks appeared at 260 nm (typical absorption of nucleic) and 280 nm (typical absorption of protein), indicating that the nucleic and protein were removed. The total sugar content in SGP was determined to be 92.98%, according to the glucose standard curve, as shown in Figure 1C. In addition, the reducing sugar content in SGP was determined to be 4.75% according to the reducing sugar standard curve, as shown in Figure 1D.

3.2 | Monosaccharide Composition and Linkage Type of SGP

In the present study, an equimolar mixture of nine monosaccharide standards (fucose, rhamnose, arabinose, galactose, glucose, xylose, fructose, galacturonic acid, and glucuronic acid) as well as the treated SGP were separated well on high-performance liquid chromatography (Figure 2A,B). Based on the chromatograms, it was determined that SGP was composed of glucose and xylose in a ratio of 98.23:1.57.

The individual peaks of partially methylated alditol acetates (PMAA) were separated well using a gas chromatography–mass spectrometer (Figure S1). The PMAA and fragmentation patterns can be identified by their mass spectra and RT. The ratios of the peak areas (total ion current) were considered the percentage of methylated sugars. The result of the methylation analysis is presented in Table 1. Five peaks were found. By comprehensively considering RT and mass fragments, the PMAA were determined to be 2,3,4,6-Me_4-Glcp; 2,4,6-Me_3-Glcp; 2,3,6-Me_3-Glcp; 2,3,4-Me_3-Glcp; and 2,4-Me_2-Glcp, with molar ratios of 0.356:0.424:0.076:0.048:0.095, respectively. The linkage type was determined to be Glcp-(1→, →3)-Glcp-(1→, →4)-Glcp-(1→, →6)-Glcp-(1→, →3,6)-Glcp-(1→ (Gao et al. 2020a; Hou et al. 2023).

3.3 | Molecular Weight of SGP

The molecular weight of SGP was determined by gel exclusion chromatography. Based on the chromatogram (Figure S2A), the calibration curve illustrated by plotting lgM_w against RT was established to calculate the molecular weight. The molecular weight of SGP was determined to be 2.64 kDa. Until then, SGP with a molecular weight of 19.037 and 33 kDa was extracted from the fruits of *S. grosvenorii* (Gong et al. 2022, 2023). The difference in molecular weight may be mainly attributed to variations in extraction and purification methods.

3.4 | Phenolic Acid Modification of SGP

Under the protection of nitrogen, Vc reacted with H_2O_2, and the resulting free radicals selectively attacked the hydroxyl hydrogens of SGP, leading to the production of macromolecular free radicals. Subsequently, phenolic acid (FA and CA) conjugated with SGP by covalent linkage to form phenolic acid–SGP (FA-SGP and CA-SGP). The molecular weight of FA-SGP and CA-SGP was determined by gel exclusion chromatography (Figure S2B,C) as 5.34 and 3.83 kDa, respectively. The result indicated that FA-SGP consisted of one mass number of SGP and 14 mass numbers of FA (grafting ratio: 50.56%), and CA-SGP consisted of one mass number of SGP and seven mass numbers of CA (grafting ratio: 31.07%). As shown in Figure 3, FA exhibited two characteristic peaks at 297 and 322 nm, and CA exhibited two characteristic peaks at 295 and 325 nm due to the π conjugations of the benzene rings in their structures. FA-SGP and CA-SGP showed

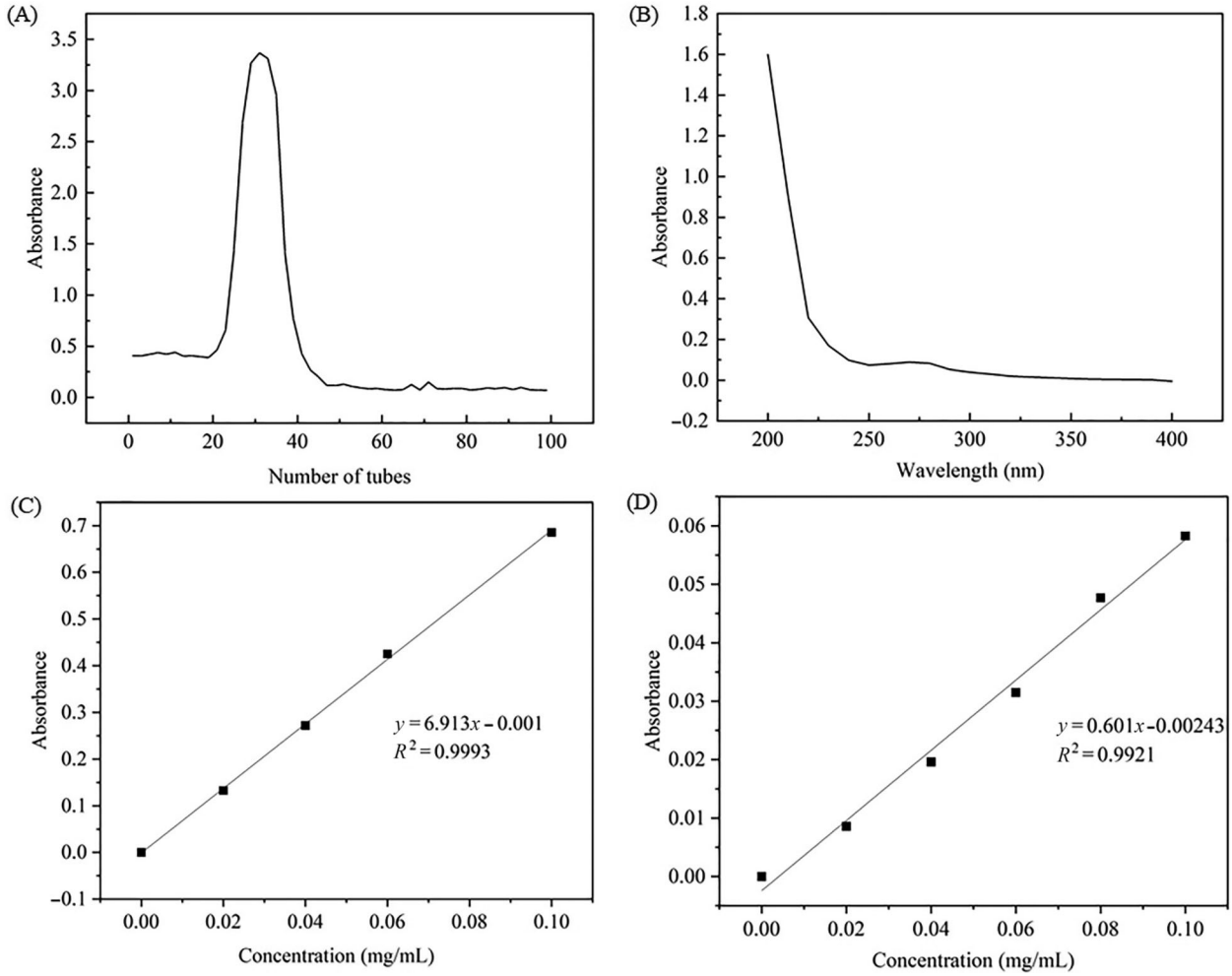


FIGURE 1 | (A) Elution curve of SGP, (B) UV spectrum of SGP, (C) glucose standard curve, and (D) reducing sugar standard curve.

two characteristic peaks similar to FA and CA, respectively, which correspond to the conjugation of the benzene rings in the moieties of phenolic acids. Compared to FA and CA, the UV characteristic peaks of FA-SGP and CA-SGP showed a slight blue shift. This may be due to the covalent bond between phenolic acids and SGP. The result indicated that FA and CA were successfully conjugated to SGP. The intensity of the absorption peak of FA-SGP slightly exceeded that of CA-SGP, suggesting a higher conjugating rate of FA-SGP in the free radical–mediated reaction. This may be because FA had a greater chance of collision with SGP due to its smaller steric hindrance. In addition, Liu et al. (2017) found that the methoxy group on the meta-position of the benzene ring in hydroxybenzoic acid could increase its reactivity. Both FA and CA are hydroxybenzoic acids. The former contains a methoxy group on the meta-position of the benzene ring, while the latter does not possess that. This may be another factor leading to a higher conjugating rate of FA-SGP in the free radical–mediated reaction.

3.5 | Surface Characteristics of SGP, FA-SGP, and CA-SGP

SEM was used to observe the microstructure of SGP, FA-SGP, and CA-SGP. The surface features were identified at 500, 1000, and 2000 fold exaggeration conditions (Figure 4). SGP existed in flaky, spherical, and rod-like structures. They were stacked on top of each other (Figure 4A), indicating that SGP possessed the main structural features of polysaccharides. In addition, SGP displayed a pore-like structure, which endowed a good hydrophilicity to the polysaccharide (Gao et al. 2020b). The FA and CA presented rectangular crystals (Figure 4B,C). The morphology of FA-SGP and CA-SGP showed a significant difference compared to native SGP, FA, and CA (Figure 4D,E). FA-SGP and CA-SGP existed in tightly interconnected reticulation structures with some folds and relatively smooth surfaces. This may be due to the reduction of inter- and intramolecular hydrogen bonding between SGP after phenolic acid modification.

3.6 | FT-IR Spectra of SGP, FA-SGP, and CA-SGP

The features of functional groups in SGP, FA-SGP, and CA-SGP were examined via FT-IR spectroscopy. As shown in Figure 5, the FT-IR spectra of SGP displayed typical polysaccharide absorption in the range of 500–4000 cm^{-1}. The distinct and broad absorption peak at 3414 cm^{-1} was assigned to the O–H stretching vibration. The small and weak absorption peak at 2930 cm^{-1} was assigned to the -CH_2 antisymmetric stretching vibration. The absorption peak at 1641 cm^{-1} was due to the asymmetric stretching vibration of the carbonyl group. The signal peaks between 800 and 1200

TABLE 1 | Glycosyl-linkage compositions of SGP.

RT (min)	Methylated sugar	Mass fragments (*m/z*)	Molar ratio	Type of linkage
16.728	2,3,4,6-Me_4-Glcp	45, 71, 87, 101, 117, 129, 145, 161, 205	0.356	Glcp-(1→
20.368	2,4,6-Me_3-Glcp	45, 87, 99, 101, 117, 129, 161, 173, 233	0.424	→3)-Glcp-(1→
21.076	2,3,6-Me_3-Glcp	45, 87, 99, 101, 113, 117, 129, 131, 161, 173, 233	0.076	→4)-Glcp-(1→
21.818	2,3,4-Me_3-Glcp	45, 87, 99, 101, 117, 129, 161, 189, 233	0.048	→6-Glcp-(1→

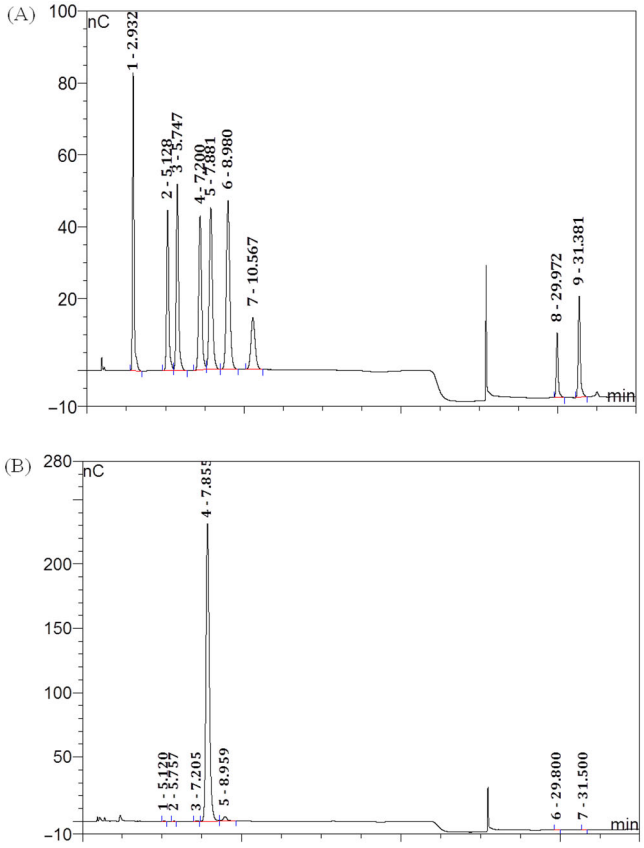


FIGURE 2 | Liquid chromatogram of (A) monosaccharide standards and (B) SGP.

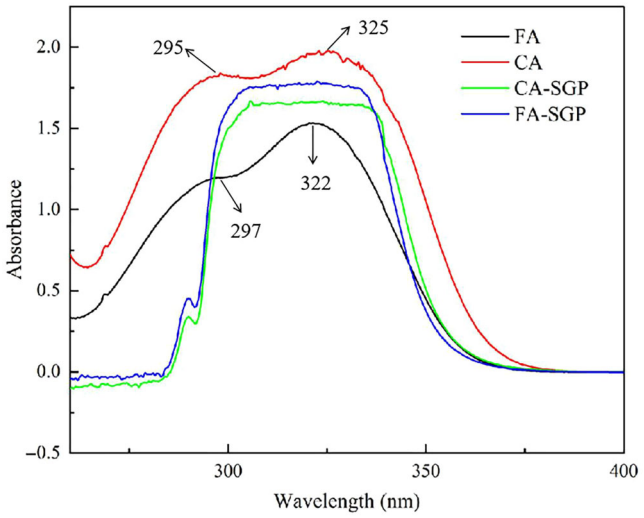


FIGURE 3 | UV spectrum of FA-SGP, CA-SGP, FA, and CA.

cm^{-1} were the fingerprint regions of carbohydrates (Xie et al. 2013). The signal at 1078 cm^{-1} was ascribed to the glucopyranose-based pyranose ring's characteristic resonance. The band at 1030 cm^{-1} suggested that the glucosyl residues were interglycosidic in the β configuration (Zhao et al. 2020). The peak at 846 cm^{-1} indicated that the SGP contained α-glycosidic bonds. Therefore, it was speculated that SGP was a pyran-type polysaccharide with both α-glycosidic and β-glycosidic bonds. Compared to SGP, the

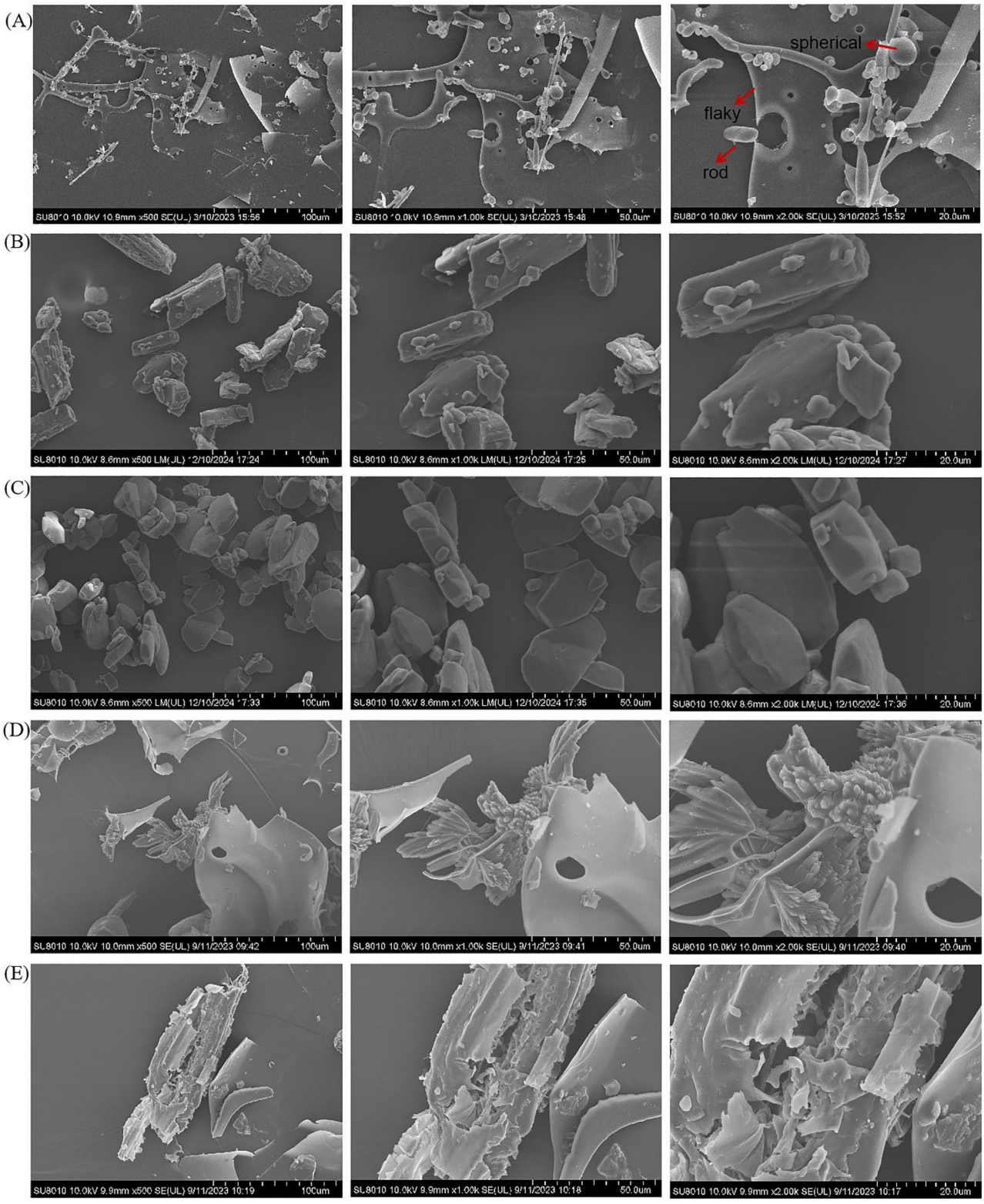


FIGURE 4 | SEM images of (A) SGP, (B) FA, (C) CA, (D) FA-SGP, and (E) CA-SGP at the magnification of 500, 1000, and 2000 folds.

FT-IR spectra of FA-SGP and CA-SGP showed new characteristic peaks at 1516 and 1526 cm^{-1}, respectively, indicating that carboxyl groups of FA and CA were covalently linked to the hydroxyl groups of SGP and formed aromatic esters. Wang et al. (2021) prepared an FA–curdlan graft copolymer and found that FA was covalently attached to curdlan through ester bonding.

3.7 | NMR Analysis of SGP, FA-SGP, and CA-SGP

The structural characteristics of SGP, FA-SGP, and CA-SGP were further analyzed by NMR spectroscopy. It was published that the chemical shift corresponding to the hydrogen proton on the heterocyclic carbon (C1) higher than 5 ppm indicated an

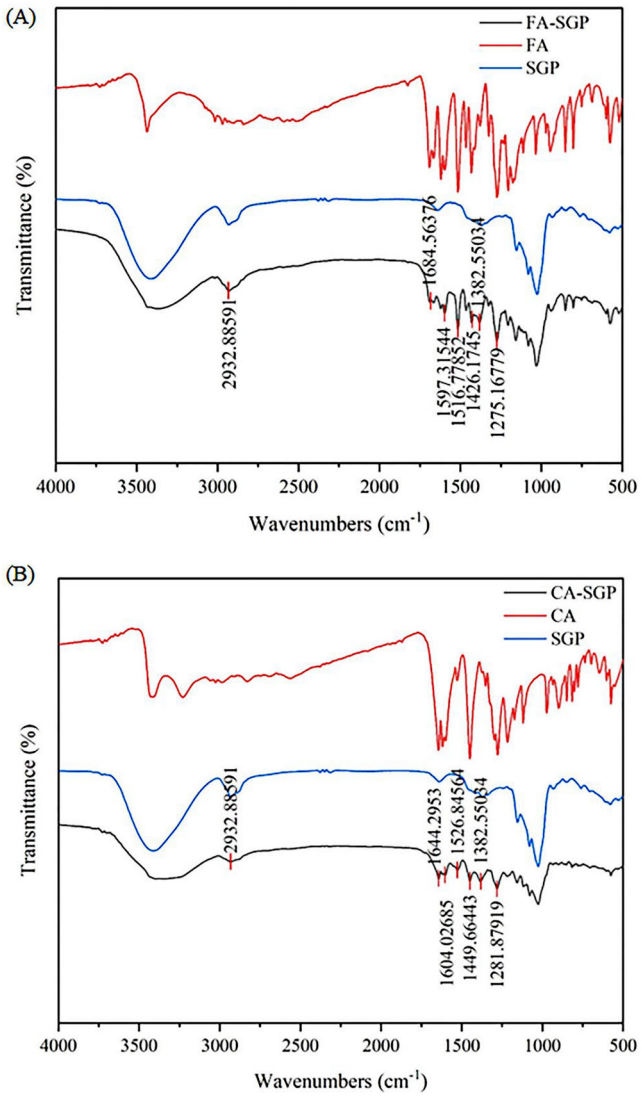


FIGURE 5 | FT-IR spectra of (A) FA-SGP group and (B) CA-SGP group.

α-glycosidic bond. Meanwhile, the chemical shift corresponding to the hydrogen proton on the C1 lower than 5 ppm indicated a β-glycosidic bond (Huang et al. 2016). The ^{1}H NMR of SGP exhibited multiple heterohead hydrogen signals in the range of δ 4.3–5.3 ppm, indicating that both α-glycosidic and β-glycosidic bonds existed in SGP. This result was consistent with that of FT-IR. Compared to SGP, the ^{1}H NMR of FA-SGP appeared to have new characteristic peaks at 6.3, 6.87, 7.0, 7.2, and 7.3 ppm, while the ^{1}H NMR of CA-SGP appeared to have new characteristic peaks at 6.3, 6.87, 7.05, 7.2, and 7.54 ppm. These new characteristic peaks in the range of δ 6.0–8.0 ppm were assigned to the hydrogen protons on the benzene rings in moieties of phenolic acids (Bunzel et al. 2003). The chemical shifts corresponding to C3 and C5 were lower than 80 ppm in ^{13}C NMR of SGP, which indicated the existence of a pyran ring (Dertli et al. 2013). The chemical shift corresponding to C1 appeared at 99.72 and 102.77 ppm, which indicated the existence of both α-glycosidic and β-glycosidic bonds (Zhong and Wang 2015). The results were consistent with those of FT-IR and ^{1}H NMR. New characteristic peaks were observed at 144, 122.4, and 116 ppm in ^{13}C NMR of FA-SGP and CA-SGP, which corresponded to the C═C of the derivatives. A new peak at 171 ppm was also found, which was attributed to the formation of the carbonyl group of the derivatives (Pasanphan et al. 2010).

3.8 | Free Radical-Scavenging Ability Analysis of SGP, FA-SGP, and CA-SGP

Radical-scavenging activity is usually used to express the antioxidant activity of natural compounds and their derivatives (Chen et al. 2019). In the present study, the DPPH• radical–scavenging activity of SGP, FA-SGP, and CA-SGP was determined. As shown in Figure 6A, SGP, FA-SGP, and CA-SGP exhibited DPPH• radical–scavenging activity in a concentration-dependent manner at 0.05–1.0 mg/mL. The results suggested that the DPPH• radical–scavenging activity of FA-SGP and CA-SGP was significant higher than that of SGP. The DPPH• radical–scavenging activity of FA-SGP, CA-SGP, and SGP at 1.0 mg/mL was 88.19 ± 0.04%, 71.42 ± 0.21%, and 23.24 ± 0.06%, respectively. The DPPH• radical–scavenging activity of FA-SGP was close to that of Vc (93.82 ± 0.04%) at 1.0 mg/mL.

OH• radicals possess extremely strong electron harvesting ability, resulting in a production of oxidation ability. The scavenging activity of SGP, FA-SGP, and CA-SGP on OH• radicals is shown in Figure 6B. SGP, FA-SGP, and CA-SGP exhibited OH• scavenging activity in a concentration-dependent manner at 0.05–1.0 mg/mL. The OH• scavenging activity of FA-SGP and CA-SGP was significantly higher than that of SGP. The OH• scavenging activity of FA-SGP, CA-SGP, and SGP at 1.0 mg/mL were 52.68 ± 1.65%, 32.27 ± 1.64%, and 26.61 ±0.30%, respectively. The scavenging activity of SGP and its derivatives was weaker than those of Vc (99.35 ± 0.02%) at all tested concentrations.

ABTS• scavenging ability assay is another fast and convenient method for evaluating antioxidant capacity. The scavenging activity of SGP, FA-SGP, and CA-SGP on ABTS• free radicals is shown in Figure 6C. SGP, FA-SGP, and CA-SGP exhibited ABTS• scavenging activity in a concentration-dependent manner at 0.05–1.0 mg/mL. The ABTS• scavenging activity of FA-SGP and CA-SGP was significantly higher than that of SGP. The ABTS• scavenging activity of FA-SGP, CA-SGP, and SGP at 1.0 mg/mL was 2.73 ± 0.04, 2.78 ± 0.02, and 2.14 ± 0.03 mM, respectively.

These findings demonstrated that FA-SGP and CA-SGP exhibited superior scavenging capacity on DPPH•, OH•, and ABTS• free radicals than native SGP. This may be because FA-SGP and CA-SGP possessed higher hydrogen donating ability. The result was consistent with previous findings suggesting that phenolic acid modification could enhance the antioxidant activity of polysaccharides (Karaki et al. 2017; Zhang et al. 2023; Xie et al. 2014). For example, Ma et al. (2019) found that FA-maltodextrin graft copolymer showed enhanced antioxidant activity compared to native maltodextrin. Wang et al. (2019) found that the antioxidant activity of CA-chitosan graft copolymer was significantly higher than that of chitosan. Although FA-SGP and CA-SGP were similar in structure, FA-SGP showed higher antioxidant activity than CA-SGP as a whole. This may be mainly attributed to the higher phenolic acid grafting ratio of FA-SGP than CA-SGP. This result was consistent with that of Liu et al. (2017).

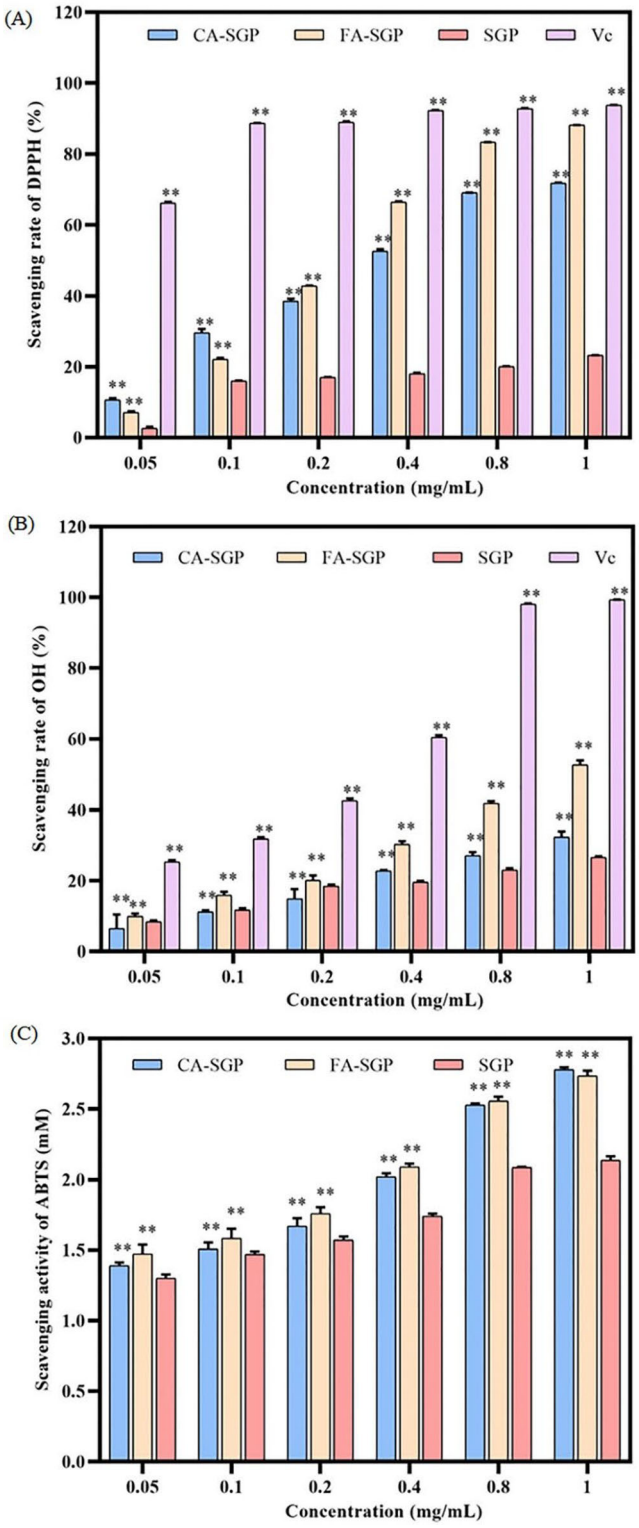


FIGURE 6 | (A) DPPH•, (B) OH•, and (C) ABTS• radical–scavenging activity of SGP, FA-SGP, and CA-SGP, $^{**}p < 0.01$, compared to SGP.

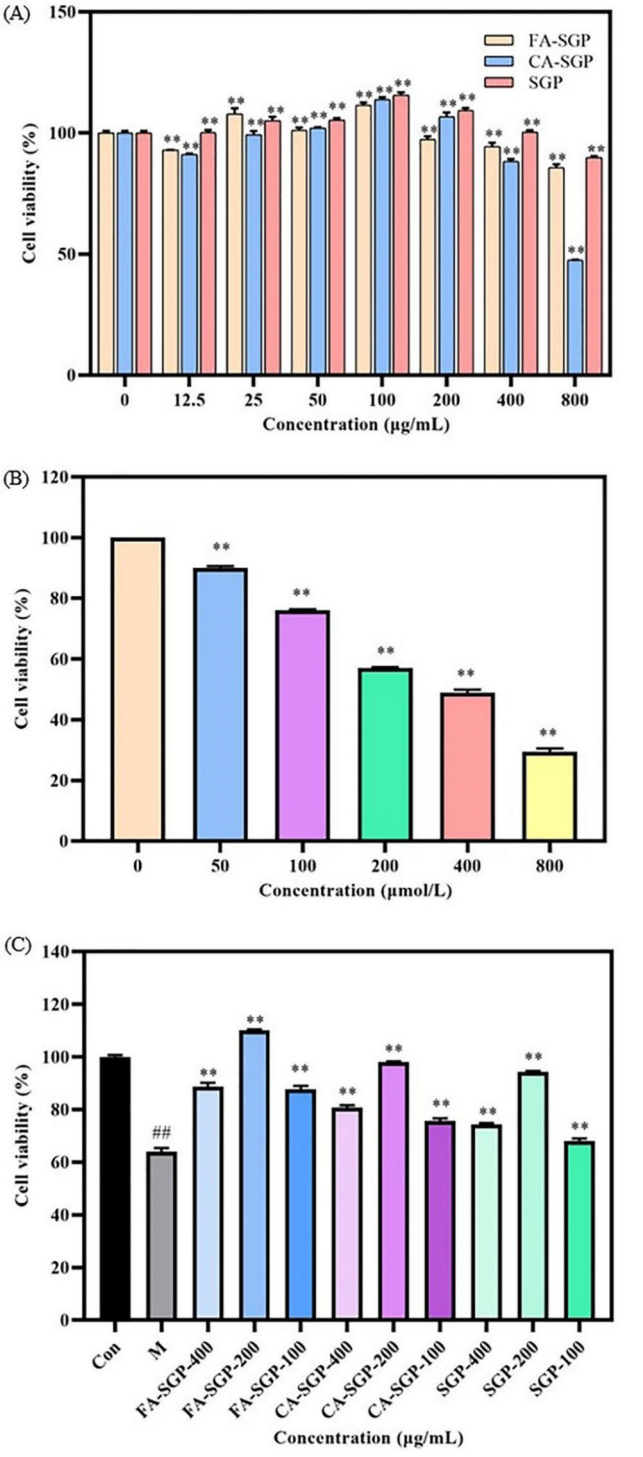


FIGURE 7 | (A) The effect of SGP, FA-SGP, and CA-SGP on healthy SH-SY5Y cell viability; (B) the effect of H_2O_2 on healthy SH-SY5Y cell viability; and (C) the protective effect of SGP, FA-SGP, and CA-SGP on H_2O_2-damaged SH-SY5Y cell. $^{\#\#}p < 0.01$, compared to control group (Con); $^{**}p < 0.01$, compared to model group (M).

3.9 | Protective Effect of SGP, FA-SGP, and CA-SGP on H_2O_2-Damaged SH-SY5Y Cells

First, the effect of SGP, FA-SGP, and CA-SGP on healthy SH-SY5Y cell viability was evaluated. As shown in Figure 7A, the cell viability of the SGP, FA-SGP, and CA-SGP treatment groups slightly increased with the increase in their concentration at 12.5–100 μg/mL. The cell viability decreased when the concentration continued to increase at 100–800 μg/mL. Thus, 100, 200, and 400 μg/mL of polysaccharides were selected as low-, medium-, and high-dose groups. Second, the optimal action concentration of H_2O_2 was selected to construct oxidative-damaged SH-SY5Y

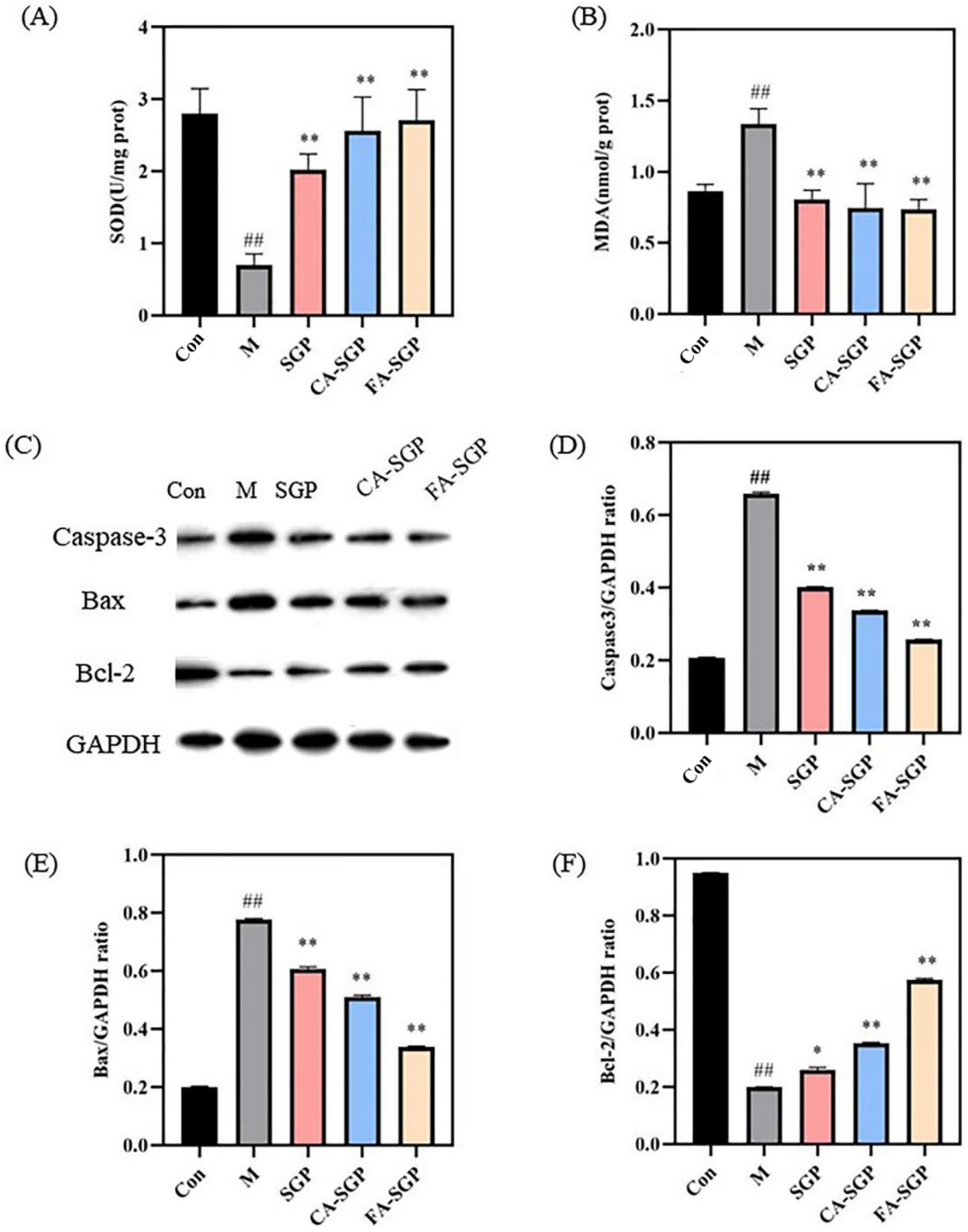


FIGURE 8 | The effect of SGP, FA-SGP, and CA-SGP toward oxidative stress in SH-SY5Y. (A) SOD; (B) MDA; (C) protein imprinting graph; (D) Caspase-3 protein expression; (E) Bax protein expression and (F) Bcl-2 protein expression. $^{\#\#}p < 0.01$, compared to control group (Con); $^{**}p < 0.01$, $^{*}p < 0.05$, compared to model group (M).

cells. As shown in Figure 7B, the cell viability of H_2O_2-treated cells decreased with an increase in its concentration at 50–800 μmol/L. The cell viability was approximately 50% at 200 μmol/L, meeting the requirement for constructing a cell model. Finally, the protective effect of SGP, FA-SGP, and CA-SGP on H_2O_2-damaged SH-SY5Y cells was evaluated. As shown in Figure 7C, SGP, FA-SGP, and CA-SGP could significantly enhance the cell viability of the H_2O_2-damaged SH-SY5Y cells under the intervention of three concentrations of 100, 200, and 400 μg/mL. The best effect was found at 200 μg/mL. FA-SGP and CA-SGP showed a higher protective effect on H_2O_2-damaged SH-SY5Y cells than on native SGP.

3.10 | Analysis of Oxidative Stress-Related Indicators and Western Blotting

Previous studies have shown that oxidative damage significantly affects intracellular antioxidant enzymes (Bai et al. 2020). SOD is an antioxidant enzyme that serves as the first line of defense for

the human body against oxidative damage (Ighodaro and Akinloye 2018). It maintains an intracellular oxidative–antioxidant balance by inhibiting oxidative damage. As shown in Figure 8A, SOD levels significantly decreased in the cells of the model group after H_2O_2 induction, while they significantly increased after SGP, FA-SGP, and CA-SGP intervention. This suggested that the intracellular antioxidant levels were enhanced by SGP, FA-SGP, and CA-SGP intervention. As substantial carbohydrate resources, polysaccharides have been reported to demonstrate antioxidant activity. Ruan et al. (2023) found that *Ulva lactuca* polysaccharide (ULP) can promote SOD activity to reduce oxidative stress.

MDA is a major secondary metabolite of lipid peroxidation formed by free radicals during oxidative stress. Its level indirectly reflects the degree of cellular damage (Xiao et al. 2008). As shown in Figure 8B, MDA levels were significantly higher in the cells of the model group than in the blank control group after H_2O_2 induction, while they significantly decreased after SGP, FA-SGP, and CA-SGP intervention. This suggested that the treatments of SGP, FA-SGP, and CA-SGP not only significantly inhibited lipid peroxidation but also reduced intracellular oxidative damage. Similarly, Zhang et al. (2024) reported that a low M_w tea polysaccharide (TPS) fraction significantly attenuated oxidative damage by decreasing MDA levels.

The Bcl-2 protein family is crucial in regulating cell apoptosis. It comprises two major categories: apoptosis-promoting proteins (e.g., Bax and Bak) and antiapoptotic proteins (e.g., Bcl-2 and Bcl-xl) (Liu et al. 2011). Caspase-3 is considered an indispensable protease in the process of apoptosis, occupying a central position in the complex biochemical network of apoptosis regulation. Many different apoptotic pathways eventually converge on the activation of Caspase-3 (Asadi et al. 2022). When cells are stimulated by proapoptotic signals such as ROS, a series of apoptotic signaling mechanisms are stimulated. Among them, the Bax protein changes the mitochondrial structure and opens the mitochondrial permeability transition pore, leading to the release of apoptotic factor cytochrome C from cells. In addition, it activates the Caspase family, initiating enzymes through apoptotic vesicle cytochrome C–dependent complexes. Caspase-3, when activated, inhibits the normal function of the antiapoptotic protein Bcl-2 and accelerates apoptosis (Chetsawang et al. 2006). In the present study, the effect of SGP, FA-SGP, and CA-SGP on the expression of three proteases Caspas-3, Bax, and Bcl-2 was revealed by western blotting analysis. As shown in Figure 8C–F, the expression levels of Caspas-3 and Bax were upregulated, and the expression level of Bcl-2 was significantly suppressed in the model group compared to the blank control group. This suggested that Caspas-3 can be activated by hydrogen peroxide stimulation, and the antiapoptotic protein Bcl-2 is inhibited, thereby accelerating apoptosis. After the intervention of SGP, FA-SGP, and CA-SGP, the expression levels of Caspas-3 and Bax were significantly downregulated, and the expression level of Bcl-2 was significantly upregulated. The results indicated that SGP, FA-SGP, and CA-SGP may alleviate the oxidative damage of H_2O_2 on SH-SY5Y cells by increasing the expression level of Bcl-2 and inhibiting the expression levels of Caspase-3 and Bax in the Bcl-2/ Caspase-3/Bax signaling pathways.

This study assessed and revealed the efficacy of the cellular antioxidant defense system with treatments of SGP, FA-SGP, and CA-SGP by measuring key biochemical indicators. These measurements revealed the effectiveness of antioxidant interventions. These results showcased their potential application in preventing and alleviating diseases related to oxidative stress.

4 | Conclusion

In summary, a novel polysaccharide was successfully isolated from the mogroside waste liquid of *S. grosvenorii*. Subsequently, two derivatives (FA-SGP and CA-SGP) were prepared by modifying native SGP with FA and CA free radical–mediated method. Structural analysis revealed that SGP was a neutral polysaccharide consisting of glucose and xylose with a molecular weight of 2.64 kDa. The linkage types were Glcp-(1→, →3)-Glcp-(1→, →4)-Glcp-(1→, →6)-Glcp-(1→, →3,6)-Glcp-(1→. The covalent linkage of FA and CA to SGP was achieved by the ester bond. The molecular weights of FA-SGP and CA-SGP were 5.34 and 3.83 kDa, respectively. Compared to native SGP, FA-SGP and CA-SGP exhibited superior scavenging capacity on DPPH•, OH•, and ABTS• free radicals and higher protective effects on H_2O_2-damaged SH-SY5Y cells. The regulation of FA-SGP and CA-SGP toward oxidative stress in SH-SY5Y cells might be related to the Bcl-2/Caspase-3/Bax signaling pathways. These findings would encourage the total utilization of *S. grosvenorii*. However, there are some limitations in the work, such as the lack of FA and CA as a control in antioxidant assays due to their poor water solubility and deep study on the mechanism of action. Further research is required to comprehensively elucidate the molecular structure–physicochemical property–functional activity relationships of FA-SGP and CA-SGP in water and lipid environments.

Author Contributions

Jiajing Duan: investigation, methodology, writing–original draft. **Yufeng Sun**: formal analysis, data curation, writing–original draft, writing–review and editing. **Bo Wang**: methodology, resources. **Qinfei Xie**: validation, visualization, software. **Yang Ju**: validation, visualization. **Fengzhong Wang**: project administration, supervision, writing–review and editing. **Bei Fan**: funding acquisition, conceptualization, supervision.

Acknowledgments

This research was supported by the National Key Research and Development Plan (2022YFD1600303, 2022YFC2010104).

Conflicts of Interest

The authors declare no conflicts of interest.

Data Availability Statement

Data will be made available on request.

References

Asadi, M., S. Taghizadeh, E. Kaviani, et al. 2022. "Caspase-3: Structure, Function, and Biotechnological Aspects." *Biotechnology and Applied Biochemistry* 69, no. 4: 1633–1645. https://doi.org/10.1002/bab.2233.

Bai, R., H. Yong, X. Zhang, J. Liu, and J. Liu. 2020. "Structural Characterization and Protective Effect of Gallic Acid Grafted O-Carboxymethyl Chitosan Against Hydrogen Peroxide-Induced Oxidative Damage." *Inter-*

national Journal of Biological Macromolecules 143: 49–59. https://doi.org/10.1016/j.ijbiomac.2019.12.037.

Bao, Y., X. Shen, and F. Wang. 2018. "The Research Progress and Development Prospects of Biosynthesis, Structure Activity Relationship and Biological Activity of Caffeic Acid and Its Main Types of Derivatives." *Natural Product Research and Development* 30, no. 10: 1825–1833+1733. https://doi.org/10.16333/j.1001-6880.2018.10.028.

Bunzel, M., J. Ralph, C. Funk, and H. Steinhart. 2003. "Isolation and Identification of a Ferulic Acid Dehydrotrimer From Saponified Maize Bran Insoluble Fiber." *European Food Research and Technology* 217, no. 2: 128–133. https://doi.org/10.1007/s00217-003-0709-0.

Chen, L., and G. Huang. 2019. "Antioxidant Activities of Phosphorylated Pumpkin Polysaccharide." *International Journal of Biological Macromolecules* 125: 256–261. https://doi.org/10.1016/j.ijbiomac.2018.12.069.

Chen, F., G. Huang, Z. Yang, and Y. Hou. 2019. "Antioxidant Activity of *Momordica charantia* Polysaccharide and Its Derivatives." *International Journal of Biological Macromolecules* 138: 673–680. https://doi.org/10.1016/j.ijbiomac.2019.07.129.

Cheng, J., J. Song, H. Wei, et al. 2020. "Structural Characterization and Hypoglycemic Activity of an Intracellular Polysaccharide From *Sanghuangporus sanghuang* Mycelia." *International Journal of Biological Macromolecules* 164: 3305–3314. https://doi.org/10.1016/j.ijbiomac.2020.08.202.

Chetsawang, B., C. Putthaprasart, P. Phansuwan-Pujito, and P. Govitrapong. 2006. "Melatonin Protects Against Hydrogen Peroxide-Induced Cell Death Signaling in SH-SY5Y Cultured Cells: Involvement of Nuclear Factor Kappa B, Bax and Bcl-2." *Journal of Pineal Research* 41, no. 2: 116–123. https://doi.org/10.1111/j.1600-079X.2006.00335.x.

Deng, Q., X. Wang, H. Chen, C. Zhao, X. Gong, and X. Zhou. 2020. "Structural Characterization, Modification and Hepatoprotective Effects of Polysaccharide From *Mori Fructus*." *International Journal of Biological Macromolecules* 153: 357–363. https://doi.org/10.1016/j.ijbiomac.2020.02.300.

Dertli, E., I. J. Colquhoun, A. P. Gunning, et al. 2013. "Structure and Biosynthesis of Two Exopolysaccharides Produced by *Lactobacillus johnsonii* FI9785." *Journal of Biological Chemistry* 288, no. 44: 31938–31951. https://doi.org/10.1074/jbc.M113.507418.

Duan, J., D. Zhu, X. Zheng, et al. 2023. "*Siraitia grosvenorii* (Swingle) C. Jeffrey: Research Progress of Its Active Components, Pharmacological Effects, and Extraction Methods." *Foods* 12, no. 7: 1373. https://doi.org/10.3390/foods12071373.

Esposito, F., C. Sinquin, S. Colliec-Jouault, et al. 2024. "Multi-Step Semi-Synthesis, Structural Characterization and Growth Factor Interaction Study of Regiochemically Sulfated Diabolican Polysaccharides." *International Journal of Biological Macromolecules* 260: 129483. https://doi.org/10.1016/j.ijbiomac.2024.129483.

Fillaudeau, A., S. Cuenot, O. Makshakova, et al. 2024. "Glycosaminoglycan-Mimetic Infernan Grafted With Poly(N-Isopropylacrylamide): Toward a Thermosensitive Polysaccharide." *Carbohydrate Polymers* 326: 121638. https://doi.org/10.1016/j.carbpol.2023.121638.

Gao, Y., Q. Guo, K. Zhang, et al. 2020a. "Polysaccharide From *Pleurotus nebrodensis*: Physicochemical, Structural Characterization and *In Vitro* Fermentation Characteristics." *International Journal of Biological Macromolecules* 165: 1960–1969. https://doi.org/10.1016/j.ijbiomac.2020.10.071.

Gao, X., H. Qu, S. Shan, et al. 2020b. "A Novel Polysaccharide Isolated From *Ulva pertusa*: Structure and Physicochemical Property." *Carbohydrate Polymers* 233: 115849. https://doi.org/10.1016/j.carbpol.2020.115849.

Gong, P., Y. Guo, X. Chen, et al. 2022. "Structural Characteristics, Antioxidant and Hypoglycemic Activities of Polysaccharide From *Siraitia grosvenorii*." *Molecules* 27, no. 13: 4192. https://doi.org/10.3390/molecules27134192.

Guo, Y., X. Chen, P. Gong, G. Li, W. Yao, and W. Yang. 2023. "The Gut-Organ-Axis Concept: Advances the Application of Gut-on-Chip Technology." *International Journal of Molecular Sciences* 24, no. 4: 4089. https://doi.org/10.3390/ijms24044089.

Gong, P., M. Wang, Y. Guo, et al. 2023. "Structure Characterization, *In Vitro* Antioxidant and Anti-Tumor Activity of Sulfated Polysaccharide From *Siraitia grosvenorii*." *Foods* 12, no. 11: 2133. https://doi.org/10.3390/foods12112133.

Hashemi, B., E. Assadpour, and S. M. Jafari. 2024. "Bigels as Novel Carriers of Bioactive Compounds: Applications and Research Trends." *Food Hydrocolloids* 147: 109427. https://doi.org/10.1016/j.foodhyd.2023.109427.

Hou, Y., J. Zhao, J. Yin, and S. Nie. 2023. "Structural Properties of *Bletilla striata* Polysaccharide and the Synergistic Gelation of Polysaccharide and Xanthan Gum." *Food Hydrocolloids* 142: 108843. https://doi.org/10.1016/j.foodhyd.2023.108843.

Hu, H., H. Li, M. Han, et al. 2020. "Chemical Modification and Antioxidant Activity of the Polysaccharide From *Acanthopanax leucorrhizus*." *Carbohydrate Research* 487: 107890. https://doi.org/10.1016/j.carres.2019.107890.

Hu, Y., J. Qiu, H. Sun, and T. Mu. 2023. "Preparation and Characterization of Caffeic Acid/Potato Starch Edible Film." *Journal of Southwest University* 45, no. 10: 72–80. https://doi.org/10.13718/j.cnki.xdzk.2023.10.008.

Huang, F., R. Zhang, Y. Liu, et al. 2016. "Characterization and Mesenteric Lymph Node Cells-Mediated Immunomodulatory Activity of Litchi Pulp Polysaccharide Fractions." *Carbohydrate Polymers* 152: 496–503. https://doi.org/10.1016/j.carbpol.2016.07.014.

Ighodaro, O. M., and O. A. Akinloye. 2018. "First Line Defence Antioxidants-Superoxide Dismutase (SOD), Catalase (CAT) and Glutathione Peroxidase (GPX): Their Fundamental Role in the Entire Antioxidant Defence Grid." *Alexandria Journal of Medicine* 54, no. 4: 287–293. https://doi.org/10.1016/j.ajme.2017.09.001.

Jin, Y., and H. Wang. 2019. "Naringenin Inhibit the Hydrogen Peroxide-Induced SH-SY5Y Cells Injury Through Nrf2/HO-1 Pathway." *Neurotoxicity Research* 36, no. 4: 796–805. https://doi.org/10.1007/s12640-019-00046-6.

Karaki, N., A. Aljawish, L. Muniglia, et al. 2017. "Functionalization of Pectin With Laccase-Mediated Oxidation Products of Ferulic Acid." *Enzyme and Microbial Technology* 104: 1–8. https://doi.org/10.1016/j.enzmictec.2017.05.001.

Li, M., X. Huang, J. Wen, et al. 2023. "Innate Immune Receptors Co-Recognition of Polysaccharides Initiates Multi-Pathway Synergistic Immune Response." *Carbohydrate Polymers* 305: 120533. https://doi.org/10.1016/j.carbpol.2022.120533.

Liu, W., L. Han, and Y. Bi. 2014. "Research Progress on the Synthesis of Caffeic Acid Derivatives." *Journal of Henan University of Technology of China* 35, no. 3: 98–104. https://doi.org/10.16433/j.cnki.issn1673-2383.2014.03.022.

Liu, J., S. Liu, Y. Chen, L. Zhang, J. Kan, and C. Jin. 2017. "Physical, Mechanical and Antioxidant Properties of Chitosan Films Grafted With Different Hydroxybenzoic Acids." *Food Hydrocolloids* 71: 176–186. https://doi.org/10.1016/j.foodhyd.2017.05.019.

Liu, J., J. Lu, J. Kan, Y. Tang, and C. Jin. 2013. "Preparation, Characterization and Antioxidant Activity of Phenolic Acids Grafted Carboxymethyl Chitosan." *International Journal of Biological Macromolecules* 62: 85–93. https://doi.org/10.1016/j.ijbiomac.2013.08.040.

Liu, X., Z. Wan, L. Shi, and X. Lu. 2011. "Preparation and Antiherpetic Activities of Chemically Modified Polysaccharides From *Polygonatum cyrtonema* Hua." *Carbohydrate Polymers* 83, no. 2: 737–742. https://doi.org/10.1016/j.carbpol.2010.08.044.

Ma, Y., Y. Feng, W. Zeng, and H. Luo. 2019. "Anthocyanin Encapsulated by Ferulic Acid-Grafted-Maltodextrin (FA-g-MD) Microcapsules Potentially Improved Its Free Radical Scavenging Capabilities Against H_2O_2-Induced Oxidative Stress." *Molecules* 24, no. 8: 1596. https://doi.org/10.3390/molecules24081596.

Mondal, S. K., B. Ray, S. Thakur, and P. K. Ghosal. 2001. "Isolation, Purification and Some Structural Features of the Mucilaginous Exudate From *Musa paradisiaca*." *Fitoterapia* 72, no. 3: 263–271. https://doi.org/10.1016/s0367-326x(00)00295-1.

Pasanphan, W., G. R. Buettner, and S. Chirachanchai. 2010. "Chitosan Gallate as a Novel Potential Polysaccharide Antioxidant: An EPR Study." *Carbohydrate Research* 345, no. 1: 132–140. https://doi.org/10.1016/j.carres.2009.09.038.

Ruan, Q., Y. Chen, J. Wen, et al. 2023. "Regulatory Mechanisms of the Edible Alga *Ulva lactuca* Polysaccharide via Modulation of Gut Microbiota in Diabetic Mice." *Food Chemistry* 409: 135287. https://doi.org/10.1016/j.foodchem.2022.135287.

Shi, M., W. Zhao, A. Yang, J. Wang, M. Xie, and C. Huang. 2024. "Preparation and Application of Phenolic Acid Compounds as Raw Materials in Cosmetics." *Fine Chemicals* 41, no. 2: 245–256+276. https://doi.org/10.13550/j.jxhg.20230222.

Tan, X., X. Zhou, and H. Chen. 2019. "Research Progress on Structure Modification of Polysaccharides." *Science and Technology of Food Industry* 40, no. 4: 341–349+356. https://doi.org/10.13386/j.issn1002-0306.2019.04.057.

Wang, Z., W. Cai, and J. Yan. 2021. "Synthetic Optimization of Ferulic Acid/Curdlan Graft Copolymers." *Modern Food Science & Technology* 37, no. 9: 179–185+185. https://doi.org/10.13982/j.mfst.1673-9078.2021.9.1100.

Wang, Y., H. Du, M. Xie, et al. 2019. "Characterization of the Physical Properties and Biological Activity of Chitosan Films Grafted With Gallic Acid and Caffeic Acid: A Comparison Study." *Food Packaging and Shelf Life* 22: 100401. https://doi.org/10.1016/j.fpsl.2019.100401.

Wang, Y., X. Li, J. Wang, T. He, C. Chi, and B. Wang. 2022. "Antioxidant Peptides From Protein Hydrolysate of Skipjack Tuna Milt: Purification, Identification, and Cytoprotection on H_2O_2 Damaged Human Umbilical Vein Endothelial Cells." *Process Biochemistry* 113: 258–269. https://doi.org/10.1016/j.procbio.2022.01.008.

Xiao, X., J. Liu, J. Hu, et al. 2008. "Protective Effects of Protopine on Hydrogen Peroxide-Induced Oxidative Injury of PC12 Cells via Ca^{2+} Antagonism and Antioxidant Mechanisms." *European Journal of Pharmacology* 591, no. 1–3: 21–27. https://doi.org/10.1016/j.ejphar.2008.06.045.

Xie, J., X. Liu, M. Shen, et al. 2013. "Purification, Physicochemical Characterisation and Anticancer Activity of a Polysaccharide From *Cyclocarya paliurus* Leaves." *Food Chemistry* 136, no. 3–4: 1453–1460. https://doi.org/10.1016/j.foodchem.2012.09.078.

Xie, M., B. Hu, Y. Wang, and X. Zeng. 2014. "Grafting of Gallic Acid Onto Chitosan Enhances Antioxidant Activities and Alters Rheological Properties of the Copolymer." *Journal of Agricultural and Food Chemistry* 62, no. 37: 9128–9136. https://doi.org/10.1021/jf503207s.

Zhang, W., M. Hadidi, A. C. Karaca, et al. 2023. "Chitosan-Grafted Phenolic Acids as an Efficient Biopolymer for Food Packaging Films/Coatings." *Carbohydrate Polymers* 314: 120901. https://doi.org/10.1016/j.carbpol.2023.120901.

Zhang, H., Q. Huang, G. Zheng, Z. Zeng, D. Xu, and K. Nong. 2019. "Effects of *Siraitia grosvenorii* Polysaccharides on Immune Function in Immunosuppressed Mice Induced by Cyclophosphamide." *Guihaia* 39: 1573–1582. https://doi.org/10.11931/guihaia.gxzw201808009.

Zhang, Z., L. Sun, R. Chen, et al. 2024. "Recent Insights Into the Physicochemical Properties, Bioactivities and Their Relationship of Tea Polysaccharides." *Food Chemistry* 432: 137223. https://doi.org/10.1016/j.foodchem.2023.137223.

Zhang, H., P. Zou, H. Zhao, J. Qiu, J. Mac Regenstein, and X. Yang. 2021. "Isolation, Purification, Structure and Antioxidant Activity of Polysaccharide From Pinecones of *Pinus koraiensis*." *Carbohydrate Polymers* 251: 117078. https://doi.org/10.1016/j.carbpol.2020.117078.

Zhang, S., Y. Zhao, Y. Wang, X. Yang, C. Chi, and B. Wang. 2022. "Gelatins and Antioxidant Peptides From Skipjack Tuna (*Katsuwonus pelamis*) Skins: Purification, Characterization, and Cytoprotection on Ultraviolet-A Injured Human Skin Fibroblasts." *Food Bioscience* 50: 102138. https://doi.org/10.1016/j.fbio.2022.102138.

Zhao, P., X. Li, Y. Wang, et al. 2020. "Characterisation and Saccharide Mapping of Polysaccharides From Four Common *Polygonatum* Spp." *Carbohydrate Polymers* 233: 115836. https://doi.org/10.1016/j.carbpol.2020.115836.

Zheng, S., Y. Wang, C. Chi, and B. Wang. 2024. "Chemical Characterization of Honeysuckle Polyphenols and Their Alleviating Function on Ultraviolet B-Damaged HaCaT Cells by Modulating the Nrf2/NF-κB Signaling Pathways." *Antioxidants* 13: 294. https://doi.org/10.3390/antiox13030294.

Zhong, L., and Z. Wang. 2015. "Effects of Yarn Polysaccharide on Antioxidant Capacity of Mice With Alzheimer Disease." *Chinese Journal of Applied Physiology* 31, no. 1: 42–48. https://doi.org/10.13459/j.cnki.cjap.2015.01.013.

Zhou, H., Y. Lin, Y. Li, et al. 2011. "Antioxidant Properties of Polymeric Proanthocyanidins From Fruit Stones and Pericarps of *Litchi chinensis* Sonn." *Food Research International* 44, no. 2: 613–620. https://doi.org/10.1016/j.foodres.2010.12.016.

Zhu, Y., L. Pan, L. Zhang, et al. 2020. "Chemical Structure and Antioxidant Activity of a Polysaccharide From *Siraitia grosvenorii*." *International Journal of Biological Macromolecules* 165: 1900–1910. https://doi.org/10.1016/j.ijbiomac.2020.10.127.

Supporting Information

Additional supporting information can be found online in the Supporting Information section.